

• Supplementary File •

Quantum key distribution over a mimicked dynamic-scattering channel

Qi-Hang Lu^{1,2}, Fang-Xiang Wang^{1,2*}, Wei Chen^{1,2,3*}, Hai-Yang Fu^{1,2,3}, Yin-Jie Lu^{1,2},
Shuang Wang^{1,2,3}, De-Yong He^{1,2,3}, Zhen-Qiang Yin^{1,2,3}, Guang-Can Guo^{1,2} & Zheng-Fu Han^{1,2,3*}

¹CAS Key Laboratory of Quantum Information, University of Science and Technology of China, Hefei, Anhui 230026, China;

²CAS Center For Excellence in Quantum Information and Quantum Physics, University of Science and Technology of China, Hefei, Anhui 230026, China;

³Hefei National Laboratory, University of Science and Technology of China, Hefei 230088, China

Appendix A The analysis of the mimicked turbulence channel

For free space QKD channel, the dynamic scattering effects (the model in Eq. 1 [1] in the main text) can be superimposed into turbulence and scattering effects. The characteristics of the turbulence effects can be quantified by the spatial and temporal parameters. The spatial parameters of the turbulence effect is related to the statistical distribution of the turbulent phase. The turbulence spectrum in Eq. 1 is defined by $\Phi_{\epsilon}^{turb}(\kappa) = 0.132C_n^2|\kappa|^{-11/3}$, where C_n^2 is the turbulence structure constant, as derived from the Kolmogorov model [8]. C_n^2 describes the spatial scale of the statistical inhomogeneity of the phase in the turbulent atmosphere. For a specific optical system, the strength of turbulence effect on the system is decided not only by C_n^2 , but also the channel length and the optical wavelength collaboratively. The Fried parameter (also called coherence length) r_0 is defined by $r_0 = (0.423k^2C_n^2L)^{-3/5}$ (L is the channel length; $k = 2\pi/\lambda$ is the optical wave number) [4], which includes the above factors and characterizes the strength of turbulence effects on a specific optical system.

The temporal characteristic can be characterized by the power spectral density (PSD) [9], which reflects the frequency components of a random series. We can characterize the time-varying feature of the turbulence effects on the optical system by analyzing the spot tilt angle PSD as follows:

$$PSD = |FFT(\theta_i)|^2, \quad (A1)$$

where θ_i denotes the tilt angle on the image of the i th time interval, and FFT is the fast Fourier transform.

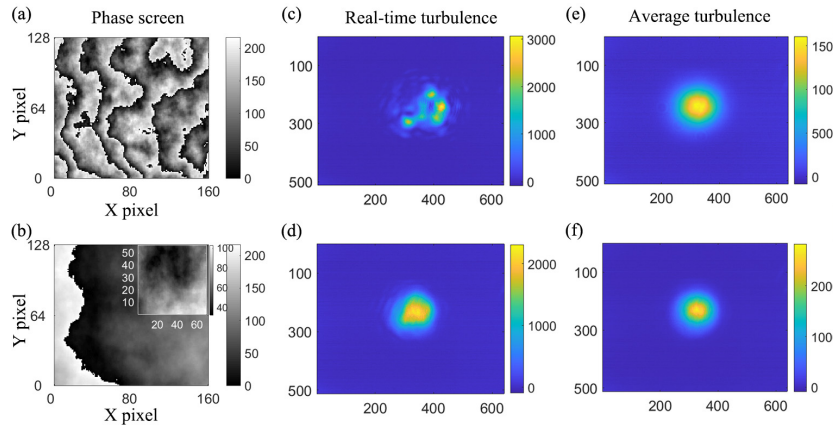


Figure A1 (a)-(b) The turbulence phase screen with coherence lengths $r_{0F} = 0.02$ m and 0.2 m, respectively. The inserted figure has an auto color bar to show the variance of the turbulence. (c)-(d) The real time spot image of Gaussian beam after passing through the turbulence screens with $r_{0F} = 0.02$ m and $r_{0F} = 0.2$ m, respectively. (e)-(f) The average spot image during the whole measurement process of the corresponding turbulent spot. All the screens above have a wind speed $N_s = 0.5$ m/s. Color bars: Pixel value. Camera exposure time: 16.7 ms. Pixel pitch on camera: $20 \mu\text{m}$

We simulate the time-variant turbulence effects by adopting the shifted-phase-screen method [6,7]. At the start of this process, we generate a static turbulence phase screen with a specific coherence length r_0 on a spatial light modulator (SLM, pixel size $12.5\mu\text{m}$, in the phase screen each 8×8 pixel block treated as a "macro pixel"), using the method proposed by C.M.Harding et al. [6]. Then, the real-time evolution of turbulence is realized by shifting the pixels of the static phase screen with a speed of N_s

* Corresponding author (email: fwxung@ustc.edu.cn, weich@ustc.edu.cn, zfhan@ustc.edu.cn)

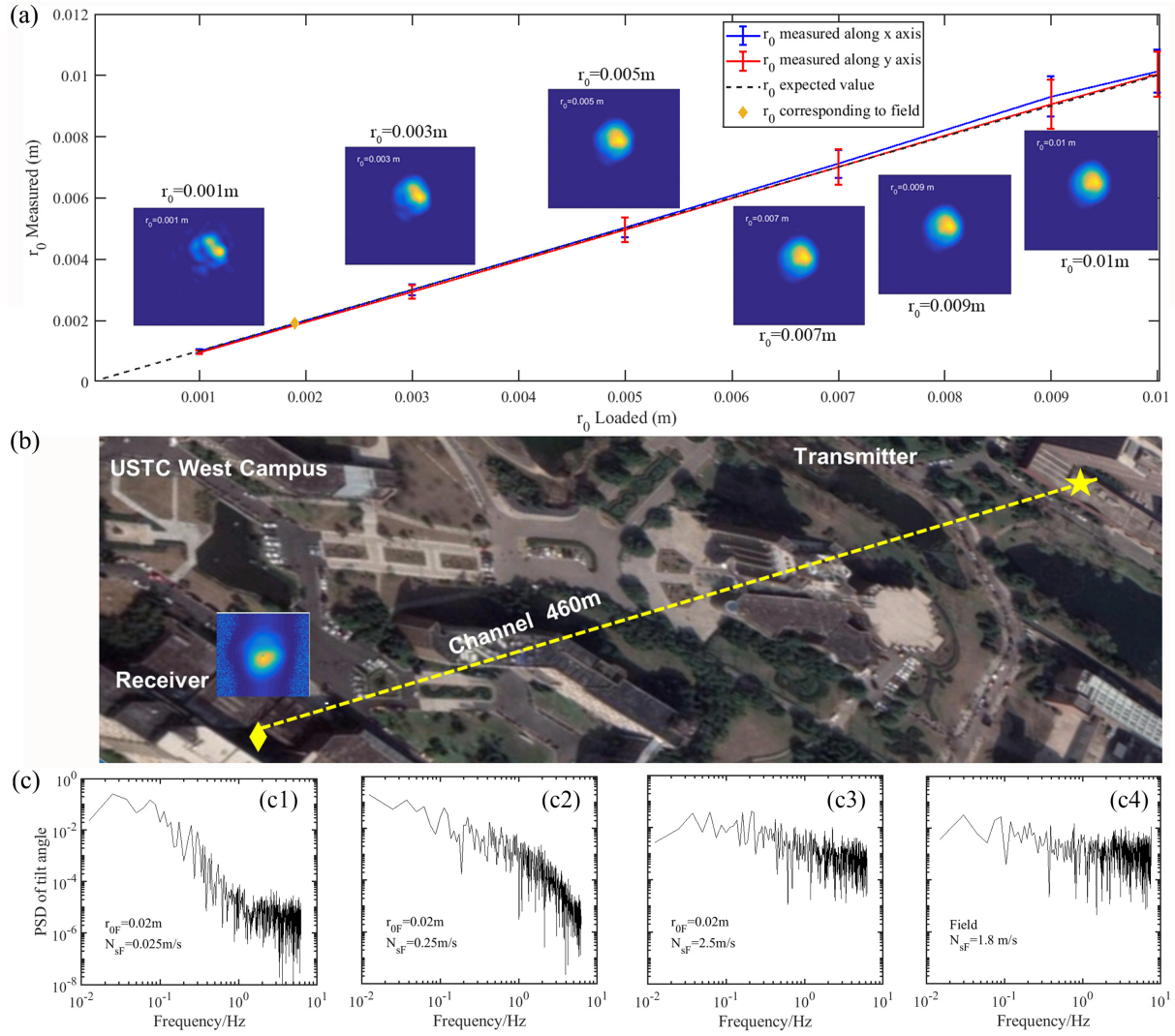


Figure A2 (a) The experimentally measured coherence length r_0 along x (blue solid line with error bar) and y (red solid line with error bar) axis versus the r_0 of the turbulence phase screens loaded on the SLM (also shown as black dashed line). The corresponding r_0 calculated from the field-test in (b) after dividing the scale factor is marked as yellow diamond. The inserted spot images show the distorted spots at each r_0 with camera pixel pitch of $20 \mu\text{m}$. (b) The field-test free space channel. The spot image is measured at the receiver with camera pixel pitch of $7.35 \mu\text{m}$. (c) The normalized time power spectral density of the beam deflection angle after passing through the turbulence phase screens with different N_{SF} under $r_{0F} = 0.02 \text{ m}$ ((c1)-(c3)) and the field channel (c4).

(defined as wind speed). To avoid emerging margins on the modulator, we implement the shifting process by generating a long phase screen at the beginning and each time taking out its part to load on the SLM. A series of the shifted phase screens are displayed sequentially with a specific frame rate to control the wind speed N_s .

The emulated channel in laboratory table is corresponded to the practical free space channel with a scale factor. According to the Fresnel-diffraction-based system scaling relation [3,4], the scaling of the optical channel length, the source diameter and other linear quantities can be related by the equation below:

$$\begin{cases} \frac{\phi_{\text{field}}}{\phi_{\text{table}}} = \sqrt{\frac{L_{\text{field}}}{L_{\text{table}}}} = A_m, \\ r_{0\text{F}} = A_m r_0, \\ N_{s\text{F}} = A_m N_s. \end{cases} \quad (\text{A2})$$

Our emulated dynamic scattering channel is $L_{\text{table}} = 1.35$ m and the diameter of the input Gaussian beam is $\phi_{\text{table}} = 3$ mm. We rescale the emulated channel to a $L_{\text{field}} = 540$ m field channel with a beam diameter of $\phi_{\text{field}} = 60$ mm, which means the scaling factor is $A_m = 20$. Accordingly, the simulated coherence length $r_{0\text{F}}$ and wind speed $N_{s\text{F}}$ of the free space channel is also 20 times of the lab channel parameters r_0 and N_s , respectively.

The characteristics of channel turbulence effects can be measured and analyzed from the spot characteristics of a laser beam after passing through the turbulence channel. The optical source of our system is a 1550 nm laser. After propagating through the turbulence channel (see Figure 1(a) in the main text, where the SLM and the propagation after it composes the turbulence channel), the spot images are taken via a CMOS camera. Figure A1(a) and A1(b) show the phase patterns corresponding to the free space channel coherence length $r_{0\text{F}} = 0.02$ m (lab $r_0 = 0.001$ m) and $r_{0\text{F}} = 0.2$ m (lab $r_0 = 0.01$ m), respectively. The real-time and time-average (long-exposure) spot images of a Gaussian beam after passing through the corresponding phase patterns are shown in Figure A1(c)-(f). Figure A2(a) shows more real-time spot images under different r_0 . It can be figured out that the smaller coherence length corresponds to the more distorted spot intensity distribution of the real-time spot and larger region of the averaged spot.

In experiment, r_0 can be calculated from the variance σ of the spot tilt angle θ at the receiver [10–12], according to the equation below [10],

$$r_0 = \left(\frac{1}{6.88} k^2 \langle \sigma^2 \rangle \right)^{-\frac{3}{5}} D^{-\frac{1}{5}}, \quad (\text{A3})$$

where D is the receiver aperture diameter. We experimentally measure the spot tilt angle from the beam centroid variance and calculate the standard variances σ of the tilt angles θ along the x and y axes, respectively. From σ the experimental coherence length r_0 can then be calculated according to Eq. A3, with D equal to the 4σ diameter [13] of the long-exposure spot in the lab channel. The experimentally measured coherence length r_0 along x and y axis in the lab channel are shown as the blue and red lines in Figure A2(a), respectively, with the error bars showing the statistical fluctuations. The measured coherence length and the coherence length of the loaded phase screens (the black dashed line in Figure A2(a)) show good agreements. The results show that our emulated channel is conform to physical reality.

To verify the effectiveness of the emulated channel with the scaling, we compare the results of the lab-emulated turbulent channel with that of a 460 m field channel (Figure A2(b), from the Science and Technology Laboratory Building to the 3rd Electrical Building in the west campus of USTC). The beam diameter and the receiver diameter in the field channel are $\phi_{\text{field}} = 60$ mm and $D = 80$ mm, respectively. The field-test data includes a series of spots at the receiver around 16:00 on Jan.12th, 2020, with temperature 5 °C, pressure 1015.2 hPa and wind speed $N_s = 1.8$ m/s. The real-time spot image at the receiver (shown in Figure A2(b)) has a spot intensity distribution which is close to that under $r_0 = 0.003$ m in the lab channel (in Figure A2(a)). In the field data, the coherence length along x axis is measured to be $r_{0\text{F}} = 0.037$ m, so it corresponds to $r_0 = 0.0019$ m in the laboratory system with a scale factor of 20 (shown as yellow diamond in Figure A2(a)).

The effectiveness of the emulated channel can be further verified temporally by the normalized PSD of the spot tilt angle, which experimentally characterizes the time-variant frequency of the turbulence. We analyze the normalized PSDs for the spot images taken after the lab-emulated turbulence channel under different wind speed $N_{s\text{F}}$ as well as in the practical field-test data, as shown in Figure A2(c). Results show that the lab-emulated turbulence under $N_{s\text{F}} = 2.5$ m/s (Figure A2(c3)) has a spot tilt angle PSD consistent with the field channel turbulence (Figure A2(c4), with the real $N_{s\text{F}} = 1.8$ m/s). The results above demonstrate that the key characteristics of the mimicked turbulence phase screens are well consistent with that of the real turbulence in the practical free space channel, which verifies the effectiveness of our channel emulation method.

Appendix B The analysis of the mimicked scattering channel

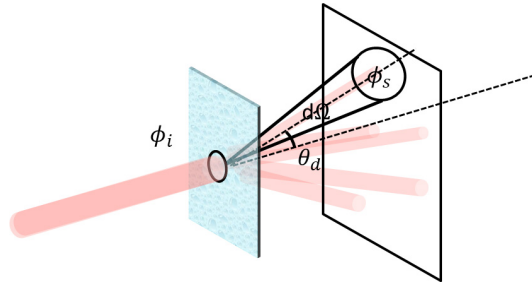


Figure B1 The model of light scattering during the measurement of the BTDF.

The characteristic of the scattering channel can be evaluated by the statistical distribution of the scattered light. In spatial frequency domain, the scattering spectrum in Eq. ?? is approximately calculated as Gaussian distribution $\Phi_{\epsilon}^{\text{scatt}}(\boldsymbol{\kappa}) =$

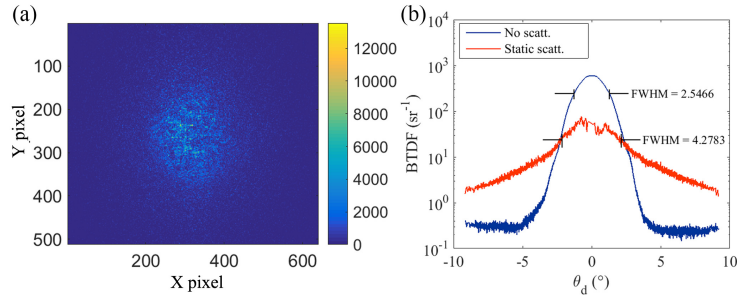


Figure B2 (a) The scattered spot of the ground glass in the channel. (b) The BTDF of the scattered spot as well as the Gaussian spot. Camera pixel pitch: $20 \mu\text{m}$. Camera exposure time: 40 ms. No scatt.: No scattering. Static scatt.: Static scattering.

$n_0 \zeta_0^4 / (8\pi k^2) \exp[-\zeta_0^2 |\kappa|^2]$, where n_0 is the mean number of scattering particles per unit volume and the parameter ζ_0 depends on the specific model and is proportional to the particle size.

In the spatial domain, the characteristic of scattering can be determined by the bidirectional scattering distribution function (BSDF) [14], which in our case is measured and calculated as the bidirectional transmission distribution function (BTDF) [5]. The BTDF is an angular-relevant function which links the scattered light in all angles with the incident light. As shown in Figure B1, with azimuthal symmetry, we can consider the influence of direction angle θ_d (the angle between the scattering direction and the propagation axis) on the BTDF function. It can be calculated as

$$\text{BTDF}(\theta_d) = \frac{\phi_s(\theta_d)}{\phi_i(\theta_d) d\Omega \cos \theta_d}, \quad (\text{B1})$$

where ϕ_s and ϕ_i are the luminous flux of the scattered and incident light at a specific direction, respectively; $d\Omega$ is the differential solid angle element and $\cos \theta_d$ is the cosine of the direction angle. In experiment, this relation can be calculated from the spot intensity distribution at different locations on the receiver plane after the scattering medium.

The scattering channel is emulated by the ground glass (polished by sand paper), which is shown in Figure ??(b). To measure and analyze the scattering characteristic of the channel, we firstly measure the spot image after the scattering channel with a CMOS camera at the receiver, as shown in Figure B2(a). It can be figured out that the spot is diffused into speckles, with the energy spread to almost the whole camera plane. Then we compare the bidirectional transmission distribution function (BTDF) of the scattered light with the Gaussian beam light. The results are shown in Figure B2(b), where BTDF distribution of the scattered light has a more flat distribution. The FWHM of the BTDF curve of the scattered light is expanded by 1.7 times relative to the Gaussian light (from 2.55 to 4.28 degree). The BTDF results demonstrate that after propagating through the scattering channel, the light energy distribution along different direction is quite diffused and the spot is highly-scattered into speckles.

As described in Section 2, the correlation between the scattered spot and Gaussian (no scattering) can reflect the variance of the spatial mode. In this experiment, the correlation is calculated to be $\text{Correlation} = 0.604$, which indicates that there is a large difference between the spatial mode of the scattered spot and the incident Gaussian spot.

Appendix C The process of the genetic algorithm

Due to its advantage of optimization robustness against the environmental noise and fluctuation, we utilize the GA to realize a wavefront-shaping module and to enhance the transmission efficiency of the optical beam through the dynamic scattering channel.

Our implementation of the GA begins with the initialization of a population of random binary modulation patterns. For each iteration, the evaluation process is performed. The modulation patterns are loaded onto the DMD. For each modulation pattern, the corresponding fitness function is measured (the received photon signals are measured by the PD and the DAQ card). After the evaluation process, the modulation patterns are suppressed and sent into the GA operation module along with the fitness function. Then the breeding process is performed. The offspring are generated by the crossing of randomly selected parents. Then the offspring are mutated with an exponentially decayed mutation rate. Once the predefined number of offspring are generated, the screens with lower fitness functions in the old population are replaced. After iterations, the whole population converges to genes with better fitness of the optimization (see Ref. [2] for more details of the GA procedure).

The fitness function in GA is used to evaluate the fitness of solution and decide the direction of the evolution. Thus, it must reflect the optimization target. In order to establish a QKD link through the dynamic scattering channel, improving the channel transmission efficiency is important. By defining the channel efficiency as the fitness function of GA the direction of the optimization will be to enhance the channel transmission efficiency and to reduce the channel loss, so the QKD process through a high-loss dynamic scattering channel can be realized.

Appendix D Setup details of the fast feedback system.

The fast-feedback optimization setup under static and dynamic scattering channel(Figure ??(b)) is mainly realized by the DMD. The DMD is placed after the BS structure to implement the wavefront optimization with amplitude modulation. The strong scattering medium is realized by the ground glass in the channel. When emulating the static scattering channel, VA1 is closed and VA2 is open. The beam passes through DMD and the ground glass. When emulating the dynamic scattering channel, VA1 is open and VA2 is closed. The beam passes through the SLM, the DMD and ground glass, successively. Due to the space limitation of the optical table, the SLM is placed before the DMD, so that the wavefront after the turbulence phase screen has sufficient length to evolve. When evolution distance is as short as 20 cm (the distance between the SLM and the DMD in Figure ?? (b)), the beam divergence is very slight, which will not influence on the optical elements of the transmitter after the SLM. After transmitting through the channel, the photons are then collected by the single mode fiber (SMF) to suppress the background noise from free-space channel. The photon signal is then detected by a photodetector (PD) and a DAQ card. The channel transmission efficiency (fitness function of the GA) is then calculated. By switching between the emulated static and dynamic scattering channels, it is then able to verify the effectiveness of the fast-feedback optimization module (also see Section 3 and Figure 4).

References

- 1 Vasylyev D, Semenov AA, Vogel W et al. Free-space quantum links under diverse weather conditions. *Phys Rev A*, 2017, 96: 043856.
- 2 Lu Q-H, Wang F-X, Huang K et al. Quantum Key Distribution Over a Channel with Scattering. *Phys Rev Applied*, 2022, 17: 034045.
- 3 Rodenburg B, Mirhosseini M, Malik M et al. Simulating thick atmospheric turbulence in the lab with application to orbital angular momentum communication. *New Journal of Physics*, 2014, 16: 033020.
- 4 Li S, Chen S, Gao C, Willner AE, Wang J. Atmospheric turbulence compensation in orbital angular momentum communications: Advances and perspectives. *Optics Communications*, 2018, 408: 68-81.
- 5 Bartell FO, Dereniak EL, Wolfe W L, et al. The Theory And Measurement Of Bidirectional Reflectance Distribution Function (Brdf) And Bidirectional Transmittance Distribution Function (BTDF). *Radiation scattering in optical systems*. SPIE, 1981, 257: 154-160.
- 6 Harding CM, Johnston RA, Lane RG. Fast simulation of a kolmogorov phase screen. *Appl Opt*, 1999, 38: 2161.
- 7 Dios F, Recolons J, Rodríguez A, Batet O. Temporal analysis of laser beam propagation in the atmosphere using computer-generated long phase screens. *Opt Express*, 2008, 16: 2206.
- 8 Kolmogorov A N. Local structure of turbulence in an incompressible viscous fluid at very high Reynolds numbers. *Soviet Physics Uspekhi*, 1968, 10(6): 734.
- 9 Goodman JW. *Statistical optics*. John Wiley & Sons, 2015.
- 10 Arteaga-Diaz P, Ocampos-Guillen A, Fernandez V. Enabling QKD under Strong Turbulence for Wireless Networks with Tilt Wavefront Correction. 2019 21st International Conference on Transparent Optical Networks (ICTON), IEEE 2019, 1-4.
- 11 Li M, Zhang P, Han J. Methods of atmospheric coherence length measurement. *Applied Sciences*, 2022, 12: 2980.
- 12 Tyson RK, Frazier BW. *Principles of adaptive optics*. CRC press, 2022.
- 13 Siegman AE. How to (Maybe) Measure Laser Beam Quality. *DPSS (Diode Pumped Solid State) Lasers: Applications and Issues*, Optica Publishing Group 1998, MQ1.
- 14 Harvey J. *Light-scattering properties of optical surfaces*. 1976.